International Journal of Solids and Structures 49 (2012) 2500–2514

Contents lists available at SciVerse ScienceDirect

International Journal of Solids and Structures

journal homepage: www.elsevier.com/locate/ijsolstr

Micromechanics based second gradient continuum theory for shear band modeling in cohesive granular materials following damage elasticity

Yang Yang [a], Anil Misra [b,*]

[a] Faculty of Mechanical and Electronic Information, China University of Geosciences, Wuhan 430074, China
[b] Civil, Environmental and Architectural Engineering Department, The University of Kansas, Lawrence, KS 66045-7609, United States

ARTICLE INFO

Article history:
Received 30 September 2011
Received in revised form 15 May 2012
Available online 7 June 2012

Keywords:
Second gradient stress–strain theory
Microstructure
Shear band localization
Cohesive materials
Granular materials
Element-Free Galerkin (EFG)

ABSTRACT

Gradient theories, as a regularized continuum mechanics approach, have found wide applications for modeling strain localization failure process. This paper presents a second gradient stress–strain damage elasticity theory based upon the method of virtual power. The theory considers the strain gradient and its conjugated double stresses. Instead of introducing an intrinsic material length scale into the constitutive law in an *ad hoc* fashion, a microstructural granular mechanics approach is applied to derive the higher-order constitutive coefficients such that the internal length scale parameter reflects the natural granularity of the underlying material microstructure. The derivations of the required damage constitutive relationships, the strong form governing equations as well as its weak form for the second gradient model are described. The recently popularized Element-Free Galerkin (EFG) method is then employed to discretize the weak form equilibrium equation for accommodating the resultant higher-order continuity requirements and further handling the mesh sensitivity problem. Numerical examples for shear band simulations show that the proposed second gradient continuum model can produce stable, accurate as well as mesh-size independent solutions without *a priori* assumption of the shear band path.

1. Introduction

Deformation localized failure mechanisms in cohesive material have been intensively studied in field of engineering computational solid mechanics for several decades due to their frequent occurrence, significance and considerable challenges. From a microscopic viewpoint, the cohesive materials in engineering are generally inhomogeneous because of the inclusion of either impurities or pre-existing micro-cracks and micro-voids. Under externally applied loads, these imperfections act as the locations that trigger the formation of shear band in the materials. As the deformation concentrates and the narrow shear band propagates, the material on either side of the dominant shear band experiences relative slip leading to the material failure. The shear bands are regarded as specific instances of the more general phenomenon of strain localization and material instability (Samaniego and Belytschko, 2005) and are important for the understanding of failure mechanisms of both brittle and ductile materials, including polymers, metals and granular materials (Rice, 1977; Bigoni and Hueckel, 1991). Upon onset of strain localization, material tangential moduli, generally, ceases to be positive-definite resulting in a set of ill-posed partial differential equations (PDE) as well as the loss of uniqueness of the solution. The consequence of such an anomalous stress–strain relationship is that the traditional finite element solutions based upon classical continuum description typically suffer from numerical instabilities, severe mesh-size and mesh-alignment sensitivities as well as zero-energy dissipation (Pietruszczak and Mroz, 1981; Bažant et al., 1984; Sandler, 1984; Frantziskonis and Desai, 1987; de Borst et al., 1993; Chen et al., 2000; Bažant, 1976; Nemes and Spéciel, 1996). In addition, the determination of the shear band propagation path remains a challenge, although a number of approaches have been advanced to address this problem.

The existing methods employed to numerically reproduce experimentally observed shear bands failure patterns generally fall into two categories based upon whether they model the shear bands as discontinuities or utilize continuum-based models. The key idea of the first type is to embed localized zones with weak or strong discontinuities into pre-determined finite elements. Examples of the weak discontinuities model include those by Rudnicki (1977), Ortiz et al. (1987), Belytschko et al. (1988), Fish and Belytschko (1988). The strong discontinuities model, which can be described as the limiting case of weak discontinuities with vanishing width, can be found in the following references (Simo et al., 1993; Simo and Oliver, 1994; Larsson et al., 1996; Armero

* Corresponding author. Address: Civil, Environmental and Architectural Engineering Department, The University of Kansas, Learned Hall, 1530 W. 15th Street, Lawrence, KS 66045-7609, United States. Tel.: +1 (785) 864 1750; fax: +1 (785) 864 5631.
E-mail address: amisra@ku.edu (A. Misra).

0020-7683/$ - see front matter © 2012 Elsevier Ltd. All rights reserved.
http://dx.doi.org/10.1016/j.ijsolstr.2012.05.024

and Garikipati, 1995, 1996; Oliver et al., 1997, 1998, 1999; Regueiro et al., 1998; Regueiro and Borja, 1999; Borja et al., 2000; Rabczuk et al., 2000; Samaniego and Belytschko, 2005; Callari et al., 2010). However, these discontinuity-based finite element strategies are not entirely satisfactory because of their inability to eliminate the spurious mesh dependency. Besides they add considerable new computational challenges, such as the difficulty of synchronizing the requisite "tracking" algorithm with the progress of multiple, inter-connected or branching discontinuities and of 3D applications (Cervera et al., 2004; Oliver et al., 2003).

Numerous efforts have also been made in the last three decades regarding the continuum-based approaches. These efforts essentially enrich the classical continuum theories with internal length scale parameters in different ways and have exhibited different efficiencies for simulating shear band failure process. These so-called regularization techniques consist of various forms of the following:

(1) The nonlocal theory which is based upon spatial averaging of tensor or scalar state variables, for example strains, stresses, or damage measures, in a certain neighborhood of a given point (Bažant et al., 1984; Belytschko et al., 1986; Bažant and Pijaudier-Cabot, 1988; Adachi et al., 1991; Valanis, 1991; Murakami et al., 1993; de Vree et al., 1995; Chen et al., 2000; Di Prisco and Imposimato, 2003; Khoei and Bakhshiani, 2005). Numerical implementation of these theories are challenging as the constitutive laws appear as convolution-type integrals accounting for the history of displacements and state variables in a finite neighborhood about the point in question.

(2) The viscoplastic theory which incorporates rate dependence or viscous effects within the constitutive models (Sandler, 1984; Wu and Freund, 1984; Needleman, 1988; Sluys and de Borst, 1992; Nemes and Spéciel, 1996). Although Needleman (1988) has suggested that the introduction of rate-dependence is sufficient to eliminate mesh sensitivity, this effect has been demonstrated only for a problem in which the width of the localization band is established *a priori*. In addition, when the material is only slightly rate-dependent problems of numerical instabilities, mesh sensitivity is still a critical issue that needs to be addressed similar to those for rate-independent models (Nemes and Spéciel, 1996).

(3) The micropolar theory which considers an additional material rotational degree of freedom independent from the displacement field (Chang and Ma, 1990; Fleck and Hutchinson, 1997; Steinmann, 1994; Su, 1994; Chang et al., 2002a,b). This approach provides an excellent means for considering scale effects and has been used successfully in the analysis of shear localization in frictional granular materials (Mohan et al., 2002) and geotechnical materials (Manzari, 2004). The theory is applicable to the cases when the rotational degree of freedom is activated during the deformation as in the case of shear dominated problems, however, the approach fails in case of pure tension (Pamin, 1994).

(4) The gradient theories which enhance the constitutive law either by introducing the strain-gradients or by including both strain-gradients and their stress conjugates (de Borst and Mühlhaus, 1992; Pamin, 1994; de Borst et al., 1995; Peerlings et al., 1996; Altan and Aifantis, 1997; Sluys, 1992; Sluys et al., 1993; Chang and Gao, 1997; Chambon et al., 1998; Chang et al., 1998; Suiker et al., 2001a,b; Chang et al., 2002; Zhao et al., 2005). The first type of gradient models have a peculiar characteristic that the discrete tangent stiffness does not maintain positive definiteness resulting in the numerical difficulties associated with strain-softening (Chang et al., 2002). In contrast, the second type of higher-order stress–strain theory appears to unconditionally maintain the stability. However, it has been rarely employed mainly because of its numerical complexity as more primary variables are added and difficulty of specifying constitutive laws as discussed in our recent paper where we have applied a similar approach to model fracture in nanoscale intergranular glassy films (Yang et al., 2011). Moreover, for certain gradient plasticity approaches there is a need for C^2 or C^1 continuity in the formulation of a finite element solution, which has impeded its application in realistic engineering problems.

Despite the above-mentioned deficiencies, gradient theories, that incorporate second or higher gradients of displacements, have emerged as appealing method for modeling strain softening behavior. The attractions of gradient methods are their simplicity as neither rotational degree of freedom nor time effects are required, nor is there any dependence on unknown 'weak zones' within the solid, and the difficult to determine influence functions for the convolution integrals appearing in the classical non-local models are avoided (Triantafyllidis and Bardenhagen, 1993). From the viewpoint of shear band modeling, there is no need to locate the incipient shear band position, or the strong/weak discontinuous line/surface, *a priori* as those for the discontinuity-based approaches (Li and Liu, 2004). In addition, this approach follows strict locality in the mathematical sense (Peerlings et al., 1996) and incorporates an inherent characteristic length scale that determines the size of the localization zone. Moreover, the gradient-enhanced models have shown to be computationally the most efficient for many materials which have low viscosity to sufficiently restore well-posedness of the boundary value problem during the strain localization phase, either in a plasticity-based format, a damage-based format, or a combination of the two (de Borst et al., 2004).

The present paper further develops the second-gradient theory (incorporating second gradients of displacements) based upon the principle of least action or the method of virtual power advanced by Germain (1973). The second gradient theory derived in this manner is not a simple generalization of the Cauchy continuum theory. The systematic application of the method of virtual power, as presented by Germain, is attractive since it leads to unambiguous formulations and physically meaningful boundary conditions (dell'Isola and Seppecher, 1995, 1997, dell'Isola et al., 2009, 2011). We apply this approach to develop the governing equations for cohesive materials undergoing damage. We then address the issues of numerical complexity and material constants associated with the practical applications of the derived second gradient theory. To this end, we develop the numerical implementation using the Element Free Galerkin (EFG) method (Belytschko et al., 1994a,b; Liu and Gu, 2005) in which approximation functions can readily satisfy the higher-order of continuity requirements. Furthermore, we derive the second gradient constitutive parameters on the basis of a microstructural granular mechanics approach (Chang and Misra, 1990; Chang and Gao, 1995; Mühlhaus and Oka, 1996). The resultant damage constitutive models incorporate the particle radius as the so-called internal length scale, to reflect the natural granularity of the underlying microstructure. Finally, the proposed second gradient continuum model is applied to simulate the shear band failure process through two 2D plane stress models to evaluate the applicability of the model.

2. Second gradient theory for material undergoing damage

The deformation energy density, W, of a second gradient continuum is assumed to be a function of the first and the second-order strain measures given as

$$W = W\left(\varepsilon^0_{ij}, \varepsilon^I_{ijk}\right); \quad \text{where } \varepsilon^0_{ij} = u_{i,j} \quad \varepsilon^I_{ijk} = u_{i,jk} \tag{1}$$

such that the conjugate stress measures are defined as

$$\sigma^0_{ij} = \frac{\partial W}{\partial \varepsilon^0_{ij}} \quad \sigma^I_{ijk} = \frac{\partial W}{\partial \varepsilon^I_{ijk}} \tag{2}$$

where σ^0_{ij} is the usual Cauchy stress and σ^I_{ijk} is termed as a double or hyper-stress. Note that all subscripts follow the summation convention of tensor unless stated otherwise. The virtual deformation energy, δE, in volume, v, of the body can be written as follows

$$\delta E = \int \left(\sigma^0_{iq} \cdot \delta\varepsilon^0_{iq} + \sigma^1_{ijq} \cdot \delta\varepsilon^1_{ijq}\right) dv \tag{3}$$

Making use of Leibnitz rule, written as,

$$\left(\sigma^1_{ijq}\delta\varepsilon^0_{ij}\right)_{,q} = \sigma^1_{ijq}\delta\varepsilon^1_{ijq} + \sigma^1_{ijq,q}\delta\varepsilon^0_{ij} \quad \text{and} \quad \left(\sigma^0_{ij}\delta u_i\right)_{,j} = \sigma^0_{ij}\delta\varepsilon^0_{ij} + \sigma^0_{ij,j}\delta u_i \tag{4}$$

along with Gauss's divergence theorem, the virtual deformation energy can be obtained as follows

$$\delta E = \int_v \left(\sigma^1_{ijq,j} - \sigma^0_{iq}\right)_{,q}\delta u_i dv - \int_{\partial v}\left(\sigma^1_{ijq,j} - \sigma^0_{iq}\right)n_q\delta u_i ds + \int_{\partial v}\sigma^1_{ijq}n_q\delta u_{i,j}ds \tag{5}$$

To further clarify the second surface integral in Eq. (5), we utilize the concept of surface divergence and the following differentiation formula (dell'Isola et al., 2012),

$$\mathrm{div}_s\left(\sigma^1_{ijq}n_q\delta u_i\right) = \sigma^1_{ijq}n_q\nabla_s(\delta u_i) + \mathrm{div}_s\left(\sigma^1_{ijq}n_q\right)\delta u_i \tag{6}$$

where ∇_s is the surface gradient operator, div_s is the surface divergence operator, and the subscript, s, pertaining to surface operators does not follow the tensor summation convention. The surface gradient of virtual displacement, δu_i, is expressed as

$$\nabla_s(\delta u_i) = \delta u_{i,j} - \delta u_{i,k}n_k n_j \tag{7}$$

Combining Eqs. (6) and (7), and applying the surface divergence theorem, we simplify the second surface integral in Eq. (5) as follows

$$\begin{aligned}\int_{\partial v}\sigma^1_{ijq}n_q\delta u_{i,j}ds &= \int_{\partial v}\sigma^1_{ijq}n_q n_j\delta u_{i,k}n_k ds - \int_{\partial v}\mathrm{div}_s\left(\sigma^1_{ijq}n_q\right)\delta u_i ds + \int_{\partial v}\mathrm{div}_s\left(\sigma^1_{ijq}n_q\delta u_i\right)ds \\ &= \int_{\partial v}\sigma^1_{ijq}n_q n_j\delta u_{i,k}n_k ds - \int_{\partial v}\mathrm{div}_s\left(\sigma^1_{ijq}n_q\right)\delta u_i ds + \int_{\partial\partial v}\sigma^1_{ijq}n_q\delta u_i v_j dl\end{aligned} \tag{8}$$

where $\partial\partial v$ represents the edge formed at the common border of two regular parts of the surface ∂v, whose outer normal vectors are n^+_q and n^-_q, and whose tangents (outward normals at the edge) are given as v^+_q and v^-_q, respectively. Thus, the virtual deformation energy in Eq. (5) becomes

$$\delta E = \int_v \left(\sigma^1_{ijq,j} - \sigma^0_{iq}\right)_{,q}\delta u_i dv - \int_{\partial v}\left[\left(\sigma^1_{ijq,j} - \sigma^0_{iq}\right)n_q + \mathrm{div}_s\left(\sigma^1_{ijq}n_q\right)\right]\delta u_i ds + \int_{\partial v}\sigma^1_{ijq}n_q n_j\delta u_{i,k}n_k ds + \int_{\partial\partial v}\sigma^1_{ijq}n_q\delta u_i v_j dl \tag{9}$$

To be consistent, the work of external forces must take the form

$$\delta L^{ext} = \int_v f_i\delta u_i dv + \int_{\partial v}T_i\delta u_i ds + \int_{\partial v}N_i\delta u_{i,k}n_k ds + \int_{\partial\partial v}R_i\delta u_i dl \tag{10}$$

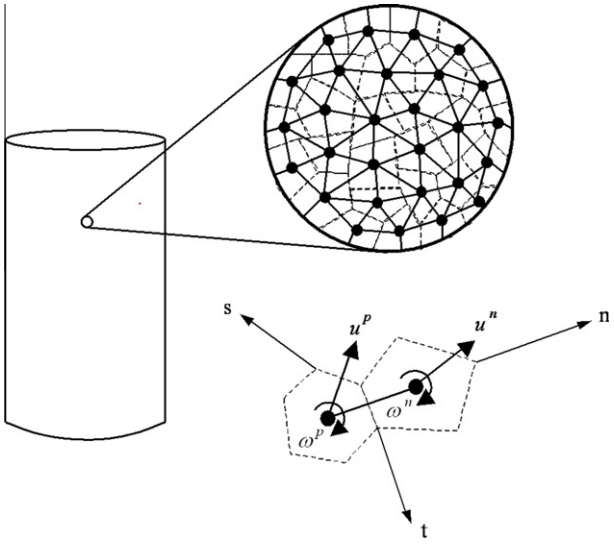

Fig. 1. Conceptual granular model of a continuum.

where we note that f_i is the body force density caused by long range interactions, T_i is the surface contact traction that expends work on surface virtual displacements, N_i is the surface contact double traction that expends work on the normal derivative of the surface virtual displacements, and R_i is the edge contact force per unit length that expends work on edge virtual displacements. We note here that a general treatment and a complete characterization of contact actions in Nth gradient continua can be found in dell'Isola et al. (2012). Now considering the principle of virtual power, we equate the internal virtual deformation energy and the work of external actions and obtain the following equilibrium equation and boundary conditions:

$$\left(\sigma^0_{iq} - \sigma^1_{ijq,j}\right)_{,q} + f_i = 0 \tag{11}$$

$$\left(\sigma^0_{iq} - \sigma^1_{ijq,j}\right)n_q - \mathrm{div}_s\left(\sigma^1_{ijq}n_q\right) = T_i \tag{12}$$

$$\sigma^1_{ijq}n_q n_j = N_i \tag{13}$$

$$\left(\sigma^1_{ijq}\right)^+ \cdot n^+_q \cdot v^+_j - \left(\sigma^1_{ijq}\right)^- \cdot n^-_q \cdot v^-_j = R_i \tag{14}$$

To proceed in a damage context, we introduce the following nonlinear second gradient constitutive damage model in which the constitutive coefficients are pre-multiplied with the same factor $(1-\omega)$ such that:

$$\sigma^0_{iq} = (1-\omega)C_{iqkl}\varepsilon^0_{kl} \tag{15}$$

$$\sigma^1_{ijq} = (1-\omega)D_{ijqklm}\varepsilon^1_{klm} \tag{16}$$

where ω is the so-called damage scalar quantity ranging from 0 for initial undamaged material to 1 when all material coherence is lost. More elaborate damage model may be considered, however for simplicity we apply the above model in this paper. For the calculations in this paper, the damage state is governed by a linear strain softening damage law through a scalar state variable, k, defined as the overall effective strain. The effective strain, k, is determined by the square root of the summation of principle strains considering damage due to only tensile strains which, in 2D, is given by the following equation

$$k = \sqrt{(\varepsilon_1)^2 + (\varepsilon_2)^2} \quad \text{for } \varepsilon_1, \varepsilon_2 > 0 \tag{17}$$

where ε_1 and ε_2 are the principal strain components of strain $\varepsilon = \begin{bmatrix}\varepsilon_{11} & \varepsilon_{12}\\ \varepsilon_{12} & \varepsilon_{22}\end{bmatrix}$. The linear softening damage evolution function takes the form

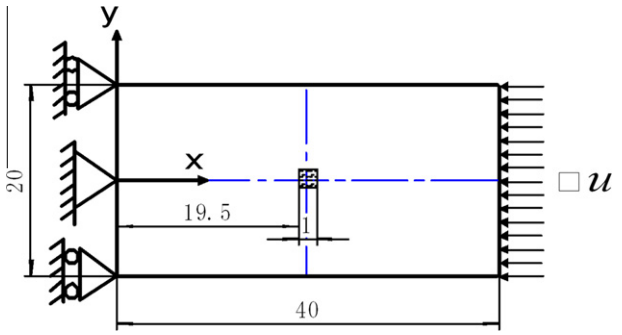

Fig. 2. Plate model with an internal imperfection–geometry and loading conditions.

$$\omega(k)=\begin{cases}0 & k<k_0\\ \frac{k_u(k-k_0)}{k(k_u-k_0)} & k_0\leqslant k\leqslant k_u\\ 1 & k>k_u\end{cases} \tag{18}$$

where k_0 is the threshold of strain at which damage is initiated and k_u is the strain level at which all load carrying capacity is exhausted. We note here that the introduced damage constitutive relationships for stress and double stress are only suitable for describing a quasi-static loading process. These expressions simply mimic the dissipative damage in the absence of unloading. However, a part of energy is indeed lost during the loading process dissipated in internal damage mechanisms. If one is interested in describing the unloading and hysteretic phenomena then the introduction of dissipation potential will be necessary (see for example, the approach discussed in Lemaitre and Chaboche (1990)– section 7.3.2 page 399 and section 7.5 page 435, for thermodynamic formulations of damage and coupled damage-plasticity models of conventional continua). We describe later in Section 4, a micromechanical derivation of the constitutive equations of type given in Eqs. (15) and (16) for cohesive material with granular microstructure whose grains are irrotational and the contact network is maintained during the deformation. The micromechanical derivation shows that the overall damage behavior is directly related to the inter-granular damage mechanism that follows the relationship given in Eq. (18).

For our further discussion, we ignore the body force f_i and substitute the damage constitutive relations from Eqs. (15) and (16) into Eq. (3) to obtain the following nonlinear equilibrium equation in terms of displacement gradients:

$$(1-\omega)[C_{iqkl}u_{k,ql}-D_{ijqklr}u_{k,rjql}]-\frac{\partial\omega}{\partial\varepsilon^0_{mn}}u_{m,qn}[C_{iqkl}u_{k,l}-D_{ijqklr}u_{k,rjl}]$$
$$+\frac{\partial\omega}{\partial\varepsilon^0_{mn}}D_{ijqklr}[u_{m,jqn}u_{k,rl}+u_{m,jn}u_{k,rql}]=0 \tag{19}$$

Pre-multiplying Eq. (17) by a test function, δu_i, and integrating over the domain, v, the weak form governing equation is obtained as follows

$$\int_v \delta u_{i,q}(1-\omega)C_{iqkl}u_{k,l}dv+\int_v \delta u_{i,qj}(1-\omega)D_{ijqklr}u_{k,rl}dv$$
$$=\int_{\partial v}T_i\delta u_i ds+\int_{\partial v}N_i\delta u_{i,k}n_k ds+\int_{\partial\partial v}R_i\delta u_i dl \tag{20}$$

where the simplification was performed following the approach used for deriving Eq. (9) since the weak form and principle of virtual work are equivalent. Additionally, the boundary integrals were simplified using the notation given in Eqs. (12)–(14). In the weak form, the terms corresponding to the test function in the boundary integrals are designated as the essential boundary conditions, while their coefficients form the natural boundary conditions (Reddy, 2005). Thus, the boundary conditions can be stated as

Essential b.c. : surface displacment u_i;
and normal derivative of suface displacment $u_{i,k}n_k$ (21)

Natural b.c. : surface forces T_i; surface double force N_i; and edge force R_i (22)

For numerical computations, the essential boundary conditions can be enforced by using penalty method as follows (Liu and Gu, 2005):

$$\int_v \delta u_{i,q}(1-\omega)C_{iqkl}u_{k,l}dv+\int_v \delta u_{i,qj}(1-\omega)D_{ijqklr}u_{k,rl}dv$$
$$-\int_{\partial v}T_i\delta u_i ds-\int_{\partial v}N_i\delta u_{i,k}n_k ds-\int_{\partial\partial v}R_i\delta u_i dl$$
$$-\frac{1}{2}\int_{\partial v}\delta[(u_i-\bar{u}_i)^T\alpha(u_i-\bar{u}_i)]ds=0 \tag{23}$$

where $\bar{u}_i$ is the prescribed displacement vector on the surface; α is the penalty coefficient which is often a large positive number. In Eq. (23), the gradient and edge essential boundary conditions are ignored for the sake of simplicity, though it can be included in an obvious and straightforward manner. Considering that

$$\frac{1}{2}\int_{\partial v}\delta[(u_i-\bar{u}_i)^T\alpha(u_i-\bar{u}_i)]ds=\int_{\partial v}\delta u_i^T\alpha u_i ds-\int_{\partial v}\delta u_i^T\alpha\bar{u}_i ds \tag{24}$$

Eq. (23) can be recast as

$$\int_v \delta u_{i,q}(1-\omega)C_{iqkl}u_{k,l}dv+\int_v \delta u_{i,qj}(1-\omega)D_{ijqklr}u_{k,rl}dv$$
$$-\int_{\partial v}\delta u_i^T\alpha u_i ds=\int_{\partial v}T_i\delta u_i ds+\int_{\partial v}N_i\delta u_{i,k}n_k ds+\int_{\partial\partial v}R_i\delta u_i dl$$
$$-\int_{\partial v}\delta u_i^T\alpha\bar{u}_i ds \tag{25}$$

3. Element-Free Galerkin (EFG) formulation

Meshfree methods, such as the EFG method and reproducing kernel particle method (RKPM), which require a much looser topological discretization structure compared to finite element method (FEM), have been used as an alternative to eliminate the mesh subjectivity as well as to simplify or avoid the time-consuming meshing task. The EFG method has been shown to be successful in solving many challenging problems in solid mechanics, for instance, static and dynamic crack growth modeling (Krysl and Belytschko, 1997, 1999; Belytschko and Tabbara, 1996; Belytschko et al., 1994a,b, 1995a,b (see also other articles coauthored by Belytschko); Lu et al., 1994; Zhang and Gao, 2010), and plate bending (Krysl and Belytschko, 1995). The gridless property also appears ideal for other problems involving moving interfaces such as solid–solid phase transformation (Cordes and Moran, 1996). The application to dynamic shear band propagation problem was conducted by Li et al. (2002) where an explicit mesh-free Galerkin formulation with RKPM kernel function has been used. Although the meshfree methods perform satisfactorily in these specific fields, they have not succeeded in replacing the finite element method (FEM). The primary reasons for the lack of wide adoption of the meshfree are (1) they are weak at representing the three-dimensional complex shapes required in practical engineering, (2) they are less reliable in terms of analysis accuracy than the FEM (Yagawa, 2004), and (3) are computationally more costly than the conventional FEM (Rajesh and Rao, 2010). In addition, the application of MLS interpolation schemes in meshfree methods complicates the imposition of essential boundary conditions as the MLS interpolants lack the delta function property of the usual FEM shape functions (Mukherjee and Mukherjee, 1997).

There have been only few attempts to apply the EFG method to gradient-enhanced continua with strain softening (Askes et al.,

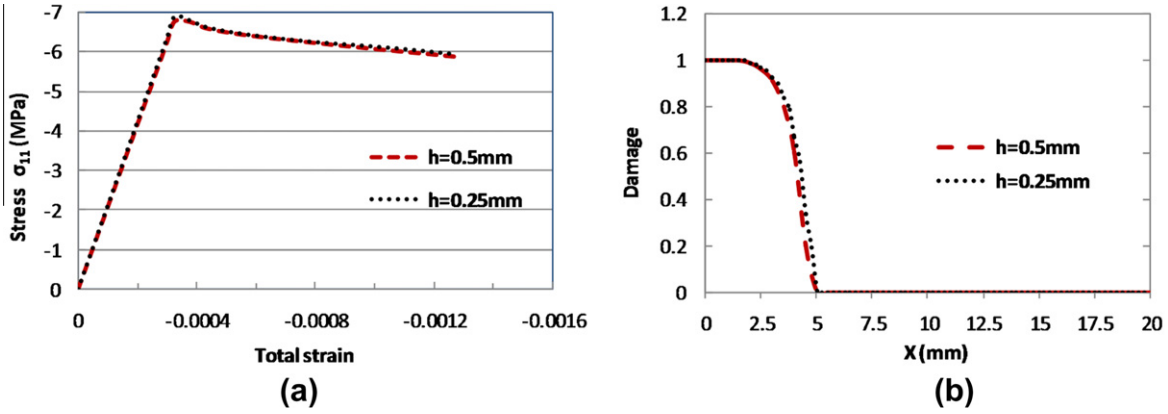

Fig. 3. Comparison between results from two different discretization schemes: (a) axial stress versus total strain curve, and (b) damage profile along horizontal axis at failure stage.

2000; Chang et al., 2002) or in the context of plasticity (Pamin et al., 2001, 2003). Jirásek (1998) has investigated the applicability of EFG method to strain softening problems and confirmed that for regularized localization problems EFG method behaves in a manner superior to FEM in the description of continuous fields. From the viewpoint of second gradient continuum theory developed in this paper, the EFG method has an important advantage over classical FEM that the approximation functions with high order of continuity needed for proper representation of the higher-order derivatives can be readily incorporated into the formulation without increasing the problem size or using projection techniques (Askes et al., 2000; Pamin et al., 2003; Rabczuk and Belytschko, 2005).

The essential idea for EFG method is that moving least square (MLS) interpolants are used for the trail and test functions with a variational principle. The connectivity between field nodes is satisfied via the overlapping of the domain of influence of sampling node in which its shape function is nonzero. The domain of influence of each field node is controlled by a weight function. A detailed description of EFG method can be found in the references (Belytschko et al., 1994a; Liu and Gu, 2005). Using MLS approximation, the trial function and test function are discretized as:

$$u_i = \phi_{ip}\underline{u}_p \quad \delta u_i = \phi_{ip}\delta\underline{u}_p \tag{26}$$

where ϕ_{ip} is the MLS shape function and $\underline{u}_p$ is the nodal parameter of displacement field for all nodes in the influence domain. Substituting Eq. (26) into the weak form Eq. (25) and canceling out $\delta\underline{u}_p$ because of its arbitrariness yields the following global discretized system equation (Yang and Misra, 2010)

$$[K_{ps} + K^{\alpha}_{ps}]\underline{u}_s = F_p + F^{\alpha}_p \tag{27}$$

where superscript α represents the resultants from penalty terms. Global stiffness tensors K_{ps}, K^{α}_{ps} and global force tensors F_p, F^{α}_p are given as

$$K_{ps} = \int_v \frac{\partial\phi^T_{ip}}{\partial x_q}(1-\omega)C_{iqkl}\frac{\partial\phi_{ks}}{\partial x_l}dv + \int_v \frac{\partial^2\phi^T_{ip}}{\partial x_q\partial x_j}(1-\omega)D_{ijqklr}\frac{\partial^2\phi_{ks}}{\partial x_r\partial x_l}dv \tag{28}$$

$$K^{\alpha}_{ps} = -\int_{\partial v}\phi^T_{ip}\alpha\phi_{is}ds \tag{29}$$

$$F_p = \int_{\partial v}\phi^T_{ip}T_i ds + \int_{\partial v}\frac{\partial\phi^T_{ip}}{\partial x_k}N_i n_k ds + \int_{\partial\partial v}\phi^T_{ip}R_i dl \tag{30}$$

$$F^{\alpha}_p = -\int_{\partial v}\phi^T_{ip}\alpha\bar{u}_i ds \tag{31}$$

We note for our calculations, the penalty parameter, α, is determined as 10^6 times the maximum diagonal element of the global stiffness matrix K.

In order to obtain the incremental form of system Eq. (27), we define a residual force R_p as the difference between internal force $(K_{ps}+K^{\alpha}_{ps})\underline{u}_s$ and external force $F_p + F^{\alpha}_p$. Taylor series expansion of the residual force is then utilized to perform the linearization given by

$$R_p = R_p(u^{(r-1)}) + \left(\frac{\partial R_p}{\partial\underline{u}_s}\right)^{(r-1)}\Delta\underline{u}^{(r)}_s + \frac{1}{2}\left(\frac{\partial^2 R_p}{\partial\underline{u}^2_s}\right)^{(r-1)}\left(\Delta\underline{u}^{(r)}_s\right)^2\cdots = 0 \tag{32}$$

where $\Delta\underline{u}^{(r)}$ is the increment and superscripts within parentheses refer to the iteration step. Thus the solution of Eq. (27) at the rth iteration can be written in terms of the solution for the $(r-1)$th iteration as follows

$$u^{(r)} = u^{(r-1)} + \Delta u^{(r)} \tag{33}$$

When second-order derivatives and higher in Eq. (32) are neglected, we obtain

$$\left(\frac{\partial R_p}{\partial\underline{u}_s}\right)^{(r-1)}\Delta\underline{u}^{(r)}_s = F_p + F^{\alpha}_p - \left(K^{(r-1)}_{ps} + K^{\alpha(r-1)}_{ps}\right)\underline{u}^{(r-1)}_s \tag{34}$$

Defining tangent stiffness as $T_{ps} = \frac{\partial R_p}{\partial\underline{u}_s}$ yields

$$T_{ps} = \sum_{m=1}^{n}\frac{\partial\left(K_{pm} + K^{\alpha}_{pm}\right)}{\partial\underline{u}_s}\underline{u}_m + \left(K_{ps} + K^{\alpha}_{ps}\right) \tag{35}$$

Inserting Eqs. (28) and (29) into Eq. (35), the resultant tangent stiffness tensor is obtained as

$$\begin{aligned} T_{ps} = {} & \int_v \frac{\partial\phi^T_{ip}}{\partial x_q}(1-\omega)C_{iqkl}\frac{\partial\phi_{ks}}{\partial x_l}dv + \int_v \frac{\partial^2\phi^T_{ip}}{\partial x_q\partial x_j}(1-\omega)D_{ijqklr} \\ & \times\frac{\partial^2\phi_{ks}}{\partial x_r\partial x_l}dv - \int_{\partial v}\phi^T_{ip}\alpha\phi_{is}ds - \int_v \frac{\partial\phi^T_{ip}}{\partial x_q}\frac{\partial\omega}{\partial\varepsilon^0_{ab}} \\ & \times\frac{\partial\phi_{as}}{\partial x_b}C_{iqkl}\varepsilon^0_{kl}dv - \int_v \frac{\partial^2\phi^T_{ip}}{\partial x_q\partial x_j}\frac{\partial\omega}{\partial\varepsilon^0_{ab}}\frac{\partial\phi_{as}}{\partial x_b}D_{ijqklr}\frac{\partial\varepsilon^0_{kl}}{\partial x_r}dv \end{aligned} \tag{36}$$

Finally, the incremental system equilibrium equation becomes

$$T^{(r-1)}_{ps}\Delta\underline{u}^{(r)}_s = F_p + F^{\alpha}_p - \left(K^{(r-1)}_{ps} + K^{\alpha(r-1)}_{ps}\right)\underline{u}^{(r-1)}_s \tag{37}$$

4. Constitutive law for second gradient media using microstructural granular mechanics

To obtain the constitutive laws for the second gradient media, macroscopic continuum is postulated to have a granular

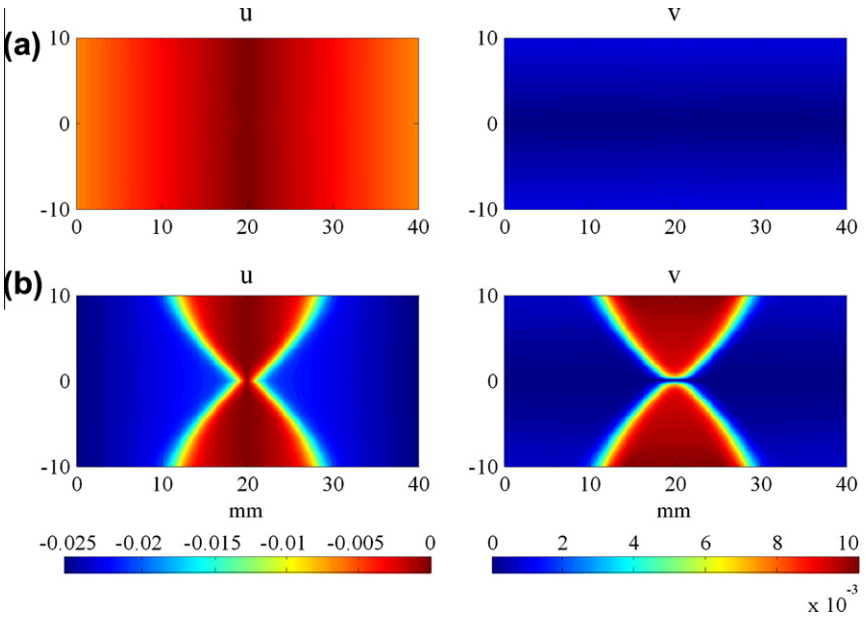

Fig. 4. Contours of horizontal and vertical displacements, denoted as u and v respectively, at (a) peak stage and (b) post-peak failure stage.

microstructure consisting of a set of interacting particles whose centroids represent material points as depicted in Fig. 1 (Misra and Yang, 2010). The term 'granular' is used here in a broad sense to describe materials that posses granular microstructures at various scales, such as ceramics and geomaterials that have been formed by particulate precursors undergoing cementation or sintering. Under an applied load on a sample of such a material, the conceptual grains may undergo translation or rotation. The relative surface displacement, δ_i, between two nearest neighbor particles $\boldsymbol{n}$ and $\boldsymbol{p}$ (Chang and Misra, 1989) is given by

$$\delta_i = u_i^n - u_i^p + e_{ijk}\left(\omega_j^n r_k^n - \omega_j^p r_k^p\right) \tag{38}$$

where u_i = particle displacement; ω_j = particle rotation; r_k = vector joining the centroid of particle to the contact point; superscripts refer to the interacting particles; e_{ijk} = the permutation symbols.

The contact force f_i^c between two particles may be related to the relative displacement δ_j^c through the contact stiffness K_{ij}^c as

$$f_i^c = K_{ij}^c \delta_j^c \tag{39}$$

with K_{ij}^c written in terms of the stiffness components in normal direction K_n and that in tangential direction K_w as

$$K_{ij}^c = K_n^c n_i n_j + K_w^c (s_i s_j + t_i t_j) \tag{40}$$

where n, s, t are the unit base vectors of the local coordinate system constructed at each contact. Vector n is normal to the contact plane and the other two orthogonal vectors, s and t, are on the contact plane which are given by

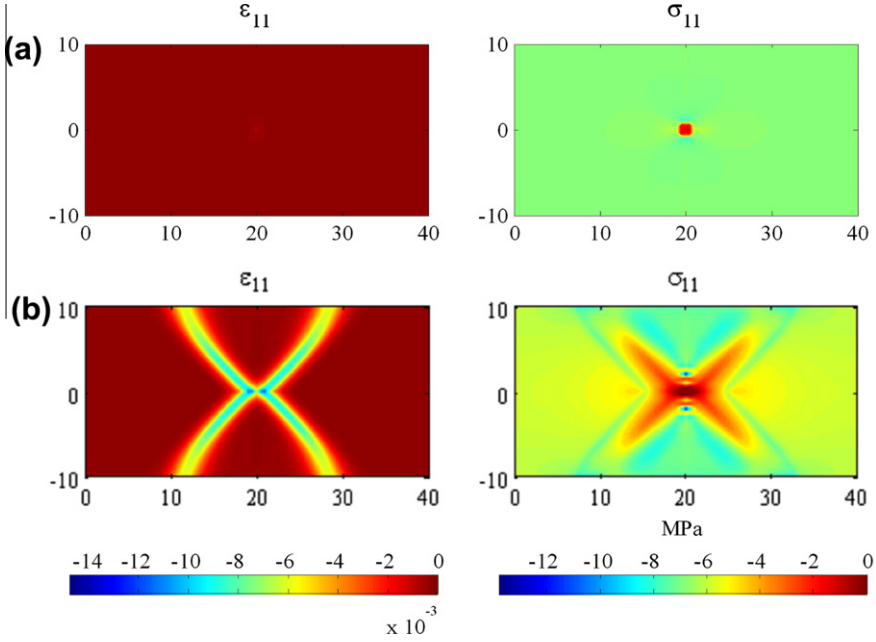

Fig. 5. Horizontal strain ε_{11} and stress σ_{11} contours at (a) peak stage and (b) post-peak failure stage.

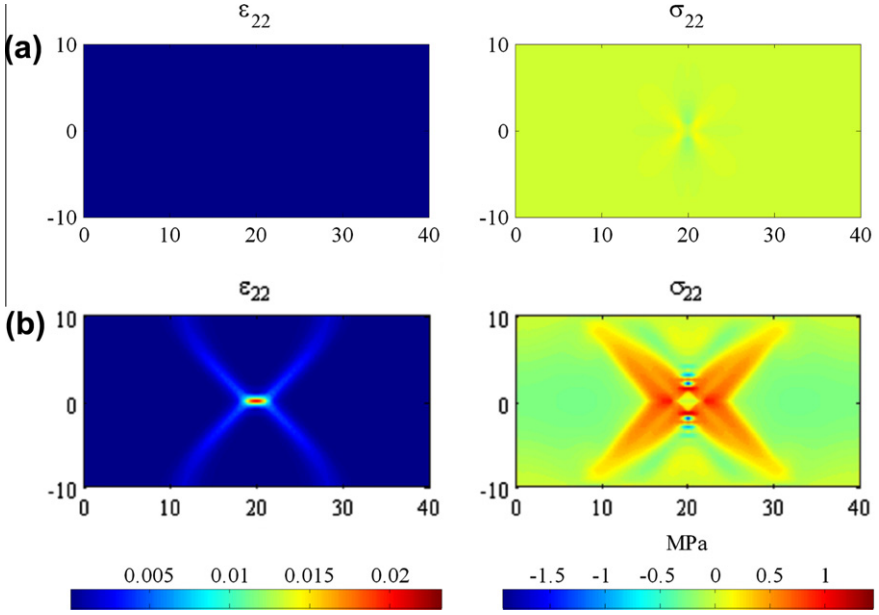

Fig. 6. Vertical strain ε_{22} and stress σ_{22} contours at (a) peak stage and (b) post-peak failure stage.

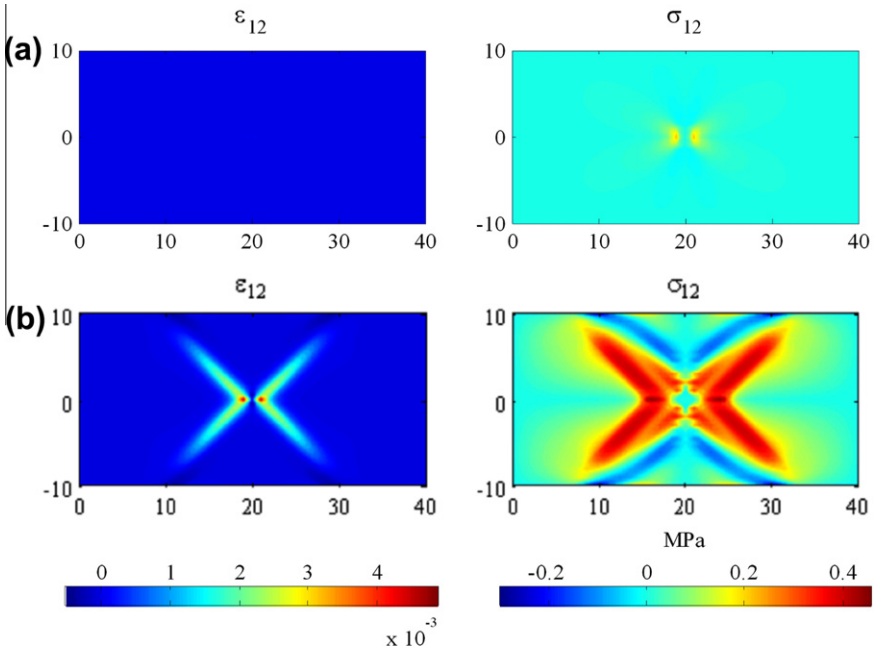

Fig. 7. Shear strain ε_{12} and stress σ_{12} contours at (a) peak stage and (b) post-peak failure stage.

$$\begin{cases} n = \cos\gamma e_1 + \sin\gamma\cos\phi e_2 + \sin\gamma\sin\phi e_3 \\ s = \frac{dn}{d\gamma} = -\sin\gamma e_1 + \cos\gamma\cos\phi e_2 + \cos\gamma\sin\phi e_3 \\ t = n\times s = -\sin\phi e_2 + \cos\phi e_3 \end{cases} \tag{41}$$

The strain energy density in a representative volume V of this pseudo-granular material can be written as

$$W = \frac{1}{2V}\sum_{c=1}^{N} f_i^c \delta_i^c \tag{42}$$

where N refers to the total number of inter-particle contacts. To develop a continuum model for the behavior of a particle assembly, we associate the discrete displacement, u_i^n, of the nth particle with the displacement of the centroid, x_i^n, of the nth particle, $u_i(x_i^n)$. Following the approach by Chang and Liao (1990), Taylor series expansions is used for the displacement field. Thus, the displacement at particle n can be estimated using the gradients at a reference point, x^0, which is taken as the barycenter of the representative volume as follows:

$$u_i(x^n) = u_i(x^0) + u_{i,j}(x^0)x_j^n + \frac{1}{2}u_{i,jk}(x^0)x_j^n x_k^n \tag{43}$$

where the derivatives of third- and higher-order are neglected. Ignoring the micro-polar effects caused by particle rotations and substituting Eq. (43) into Eq. (38) we get

$$\delta_i^c = u_i(x^n) - u_i(x^p) = u_{i,j}L_j^c + u_{i,jk}J_{jk}^c \tag{44}$$

where the geometric quantities

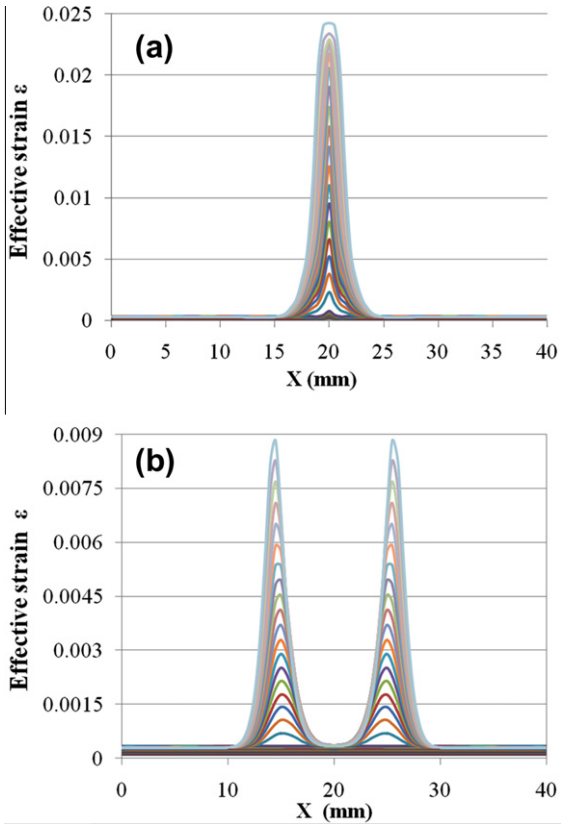

Fig. 8. Effective strain ε evolution with loading at (a) along the horizontal central axis (y = 0), and (b) along the horizontal axis (y = 5 mm) of the plate.

$$L_j^c = x_j^n - x_j^p \tag{45a}$$

$$J_{jk}^c = \frac{1}{2}\left(x_j^n x_k^n - x_j^p x_k^p\right) \tag{45b}$$

Assuming that the pseudo-particle radius is uniform denoted by, r, Eqs. (45a) and (45b) are reduced to

$$L_j^c = 2rn_j^c \tag{46a}$$

$$J_{jk}^c = \frac{1}{2}L_j^c L_k^c \tag{46b}$$

By combining Eqs. (38), (39), (44), and (46), following constitutive tensors are obtained for the case of material with central symmetry:

$$C_{ijqm} = \frac{1}{2V}\sum_{c=1}^{N} L_j^c K_{iq}^c L_m^c \tag{47a}$$

$$D_{ijkqmn} = \frac{1}{8V}\sum_{c=1}^{N} L_j^c L_k^c K_{iq}^c L_m^c L_n^c \tag{47b}$$

Considering the symmetry of the stress and strain tensors, the fourth-rank and sixth-rank constitutive tensors have to satisfy the following symmetries

$$C_{ijkl} = C_{klij}; \quad C_{ijkl} = C_{jikl} = C_{ijlk} \tag{48}$$

$$D_{ijqklm} = D_{klmijq}; \quad D_{ijqklm} = D_{jiqklm} = D_{ijqlkm} \tag{49}$$

Since the representative volume consists of a large number of particles, a summation of any quantity over all particle contacts within the volume can be expressed in an integral form by introducing a directional density function, $\xi(\gamma,\phi)$ (Chang and Misra, 1990). For a suitably large representative volume with a large number of contacts, recalling Eq. (46a), the summation in Eqs. (47a) and (47b) may be recast into integral forms as

$$C_{ijkl} = \frac{2r^2 N}{V}\int_{\Omega} n_j^c K_{ik}^c n_l^c \xi(\gamma,\phi)d\Omega \tag{50a}$$

$$D_{ijqklm} = \frac{2r^4 N}{V}\int_{\Omega} n_j^c n_q^c K_{ik}^c n_l^c n_m^c \xi(\gamma,\phi)d\Omega \tag{50b}$$

where the integration $\int_\Omega(\,)d\Omega = \int_0^{2\pi}\int_0^{\pi}(\,)\sin\gamma d\gamma d\phi$; and $N\xi(\gamma,)\phi\, d\Omega$ = the number of contacts in the interval Ω to $\Omega + d\Omega$. Since the representative volume is much larger compared to the particle radius, r, the higher order constitutive constants, D_{ijqklm}, are generally order of magnitude smaller than the conventional constitutive constants, C_{ijkl}. However, in the presence of large strain gradients as those in the shear bands, these play a significant role. We further note that the micro–macro identification which is proposed and used here produces a relevant second gradient effect because of

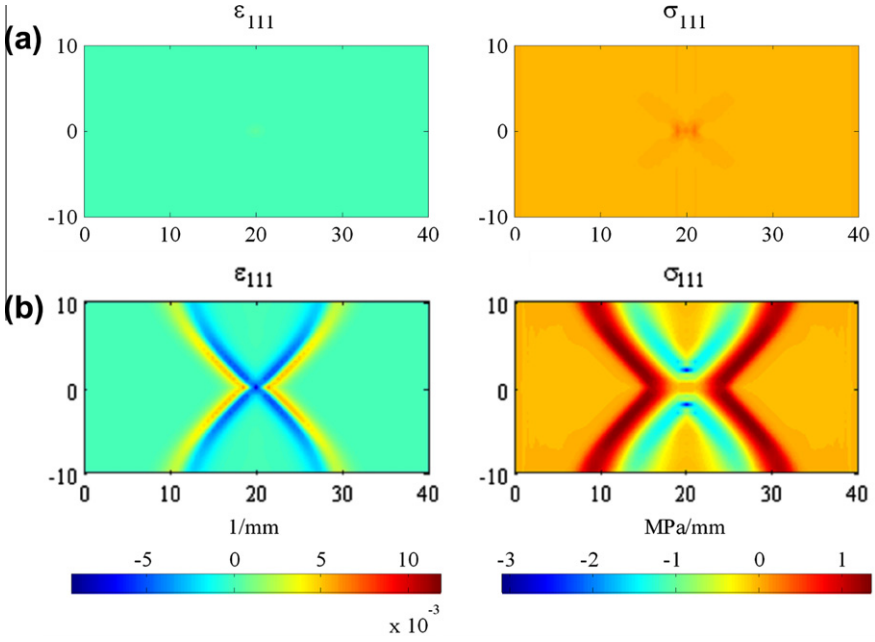

Fig. 9. Higher-order strain ε_{111} and stress σ_{111} contours at (a) peak stage and (b) post-peak failure stage.

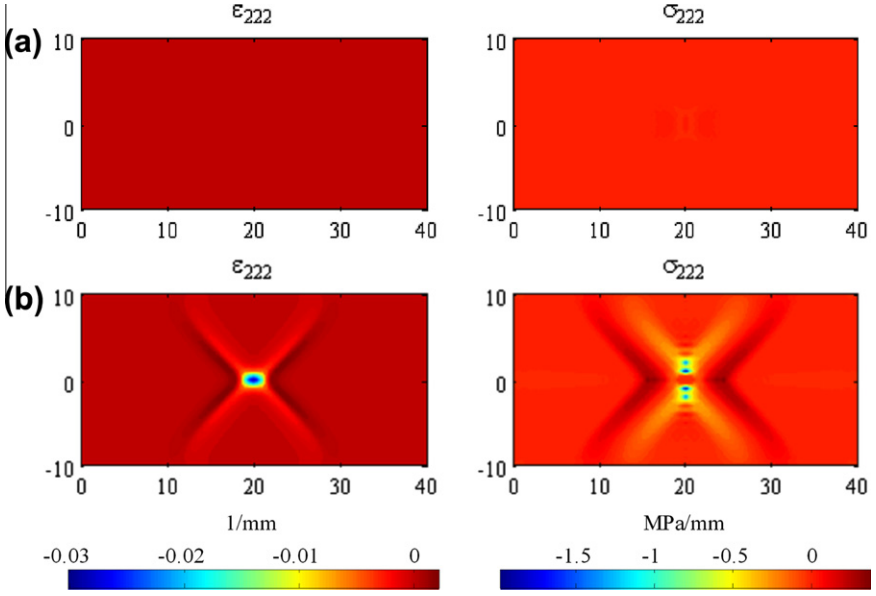

Fig. 10. Higher-order strain ε_{222} and stress σ_{222} contours at (a) peak stage and (b) post-peak failure stage.

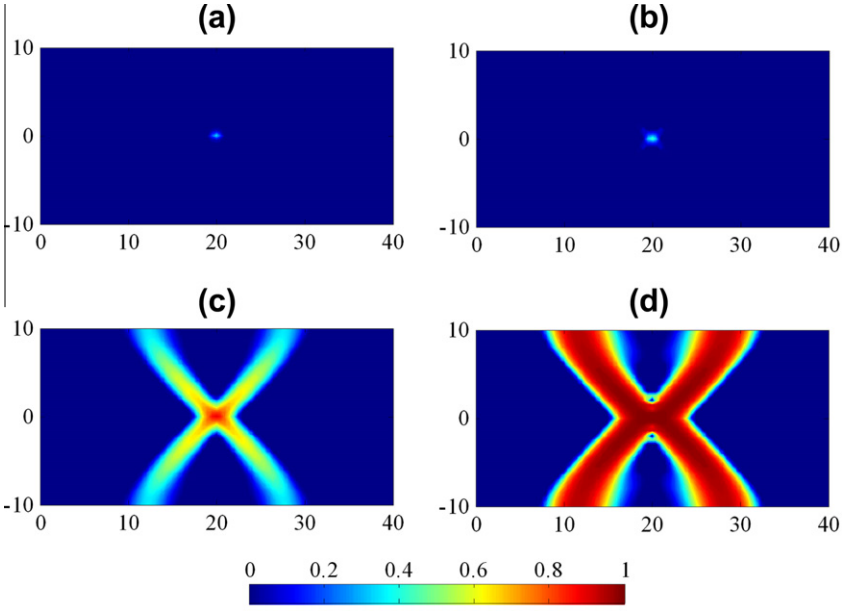

Fig. 11. Damage evolution process at selected overall displacement levels of (a) −0.006 mm, pre-peak, (b) −0.0065 mm, peak, (c) −0.0075 mm, post-peak pre-failure, (d) −0.0255 mm, post-peak failure.

the presence of strong non-linearities in the interactions at the microscopic level. Instead the same effect is obtained in systems in which at microlevel the interaction forces are linear, but strong space variation of elastic properties are observed (Alibert et al., 2003; Seppecher et al., 2011).

Now, for an isotropic microstructure, the directional density function is given as

$$\xi(\gamma,\phi)=\frac{1}{4\pi} \tag{51}$$

and closed form expressions for the constitutive coefficients can be derived in terms of the Young's modulus, Poisson's ratio and the particle size. Substituting Eqs. (40), (41) and (51) into (50a) and integrating we arrive at the constitutive constants, C_{ijkl}, as

$$C_{1111}=\frac{a}{15}(3K_n+2K_w) \tag{52a}$$

$$C_{1122}=\frac{a}{15}(K_n-K_w) \tag{52b}$$

$$C_{1212}+C_{1221}=\frac{a}{15}\left(K_n+\frac{3}{2}K_w\right) \tag{52c}$$

where $a=2r^2\,N/V$ represents the density of the packing structure. In addition, the following identities for elastic moduli hold:

$$C_{1111}=C_{2222};\quad C_{1122}=C_{2211};\quad C_{1212}=C_{2121} \tag{53}$$

The constitutive constants results in the following relations between material properties and components of pseudo-bond stiffness (Chang and Misra, 1990):

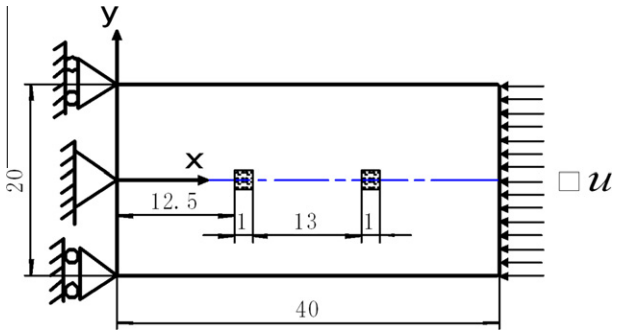

Fig. 12. Plate model with two internal imperfections– geometry and loading conditions.

$$E = a\left(\frac{K_n(2K_n + 3K_w)}{3(4K_n + K_w)}\right) \tag{54}$$

$$v = \frac{K_n - K_w}{4K_n + K_w} \tag{55}$$

Eqs. (54) and (55) can be rearranged to give the pseudo-bond stiffness

$$K_n = \frac{3E}{a(1-2v)} \tag{56}$$

$$K_w = \frac{3E(1-4v)}{a(1-2v)(1+v)} \tag{57}$$

By combining Eqs. (40), (41), (50b), (51), (56) and (57) and using a similar algebra, the components of second gradient constitutive constants D_{ijqklm} can be obtained as

$$D_{111111} = \frac{3r^2E(7-3v)}{35(1-2v)(1+v)} \tag{58a}$$

$$D_{111122} = \frac{r^2E(7-13v)}{35(1-2v)(1+v)} \tag{58b}$$

$$D_{111212} = \frac{3r^2Ev}{7(1-2v)(1+v)} \tag{58c}$$

$$D_{122122} = \frac{3r^2E(7-23v)}{35(1-2v)(1+v)} \tag{58d}$$

where the following relations hold

$$D_{111111} = D_{222222} \tag{59a}$$

$$D_{111122} = D_{112112} = D_{112121} = D_{121121} = D_{211222} = D_{212212} = D_{212221} = D_{221221} \tag{59b}$$

$$D_{111212} = D_{111221} = D_{112211} = D_{112222} = D_{121211} = D_{121222} = D_{122212} = D_{122221} \tag{59c}$$

$$D_{122122} = D_{211211} \tag{59d}$$

The other elements of C_{ijkl} and D_{ijqklm} are all zero. Note that: (1) Eq. (58) provides a useful method for estimating the high-order constitutive constants directly from the Young's modulus and Poisson's ratio without explicitly knowing the numerical values of either the number of contacts N or the representative volume V; and (2) the derived higher-order constitutive coefficients explicitly depend upon the particle radius, r, which acts as a internal length scale parameter. Furthermore, the direct relationship between the pseudo-bond stiffness and the overall properties provides a way to relate the grain-scale damage to the overall material damage as discussed in Misra and Yang (2010). For example in this paper, we model damage as a loss of stiffness of the pseudo-bonds by multiplying the stiffness in Eqs. (56) and (57) with the factor $(1-\omega)$ where the scalar damage parameter, ω, is given in Eq. (18). It is straightforward to show that the resultant coefficients in Eqs. (52) and (58) are of the same form as the constitutive law assumed in Eqs. (15) and (16). Thus the overall damage behavior of the material is directly related to the damage mechanism (and the accompanying dissipation) at the pseudo-bonds.

5. Application to shear band failure simulation

Shear band simulations have been widely studied as benchmark problems by many researchers to assess their numerical models. Cervera et al. (2004) modelled shear band localization for three 2D perforated strip examples with different perforations in order to evaluate their stabilized isotropic local J_2 damage constitutive model. Li and Liu (2004) used different shear band simulation approaches to investigate frequently encountered problems including mesh-alignment sensitivity, controllability of hour-glass modes and adaptive analysis. In this paper, the applicability of

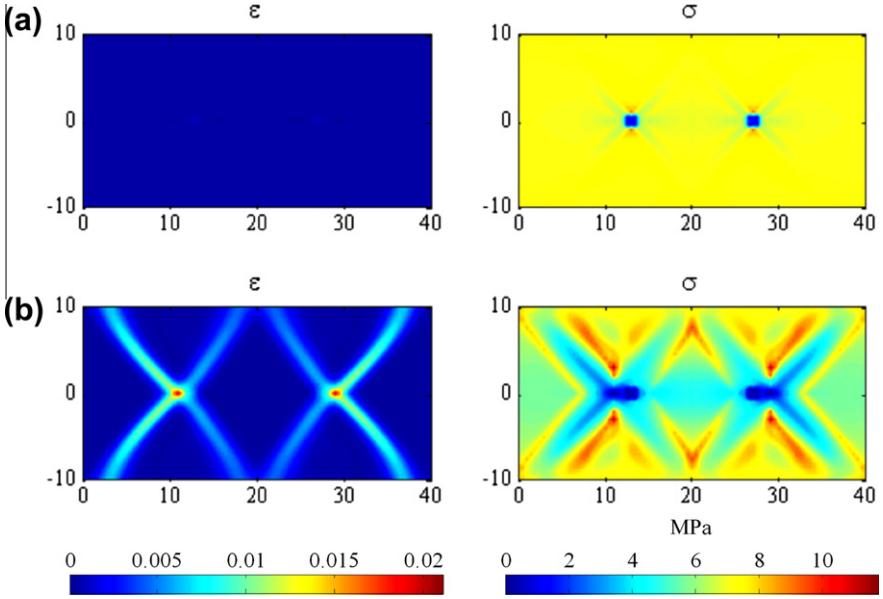

Fig. 13. Effective strain ε and stress σ contours at (a) peak stage and (b) post-peak failure stage.

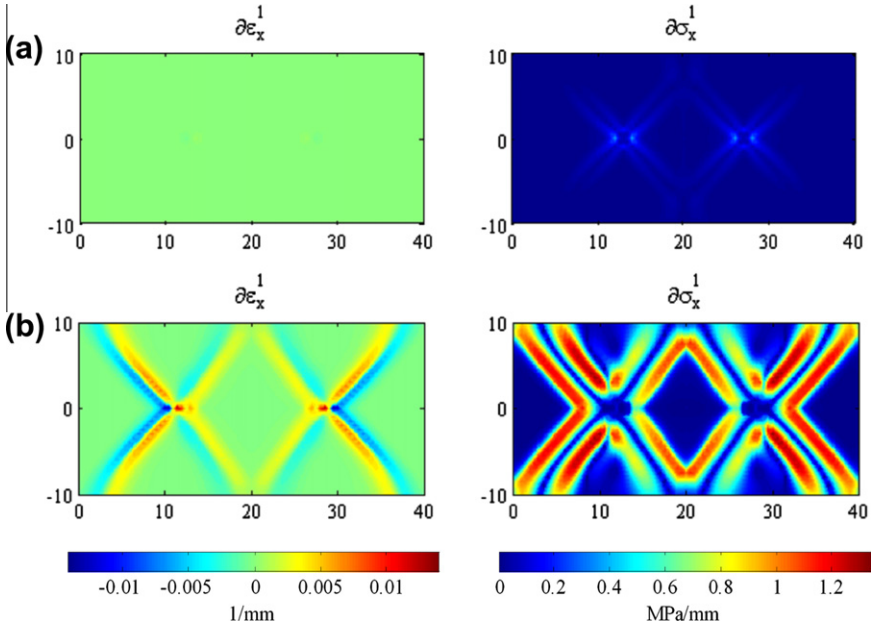

Fig. 14. Contours of the overall effective higher-order strain gradient and conjugated stress in *x*-direction at (a) peak stage and (b) post-peak failure stage.

the developed second gradient continuum model is illustrated through two benchmark 2D numerical examples for shear band simulation.

5.1. Plate with single imperfection

In the first example we simulate shear band formation in a 2D plate model of dimension 40 mm × 20 mm subjected to a displacement-controlled compressive loading in the *x*-direction as shown in Fig. 2, while the boundaries in the *y*-direction are kept traction free. To initiate shear localization, a square imperfection with side length of 1 mm was placed at the central zone of the plate. Fig. 2 depicts the undeformed plate geometry and its boundary conditions, in which the hatched area represents the imperfection. The Young's modulus of plate was taken as $E = 20$ GPa, the Poisson's ratio $\nu = 0.22$, internal length scale parameter $r = 0.5$ mm and the damage evolution parameters, $k_0 = 10^{-4}$ and $k_u = 0.0125$. The imperfection is characterized by 80% reduction of the Young's modulus.

Considering the symmetry of both the geometry and the boundary conditions, the top right quarter of the plate was analyzed. Two cases of model discretizations were considered. In case 1, a total of 861 (41×21) regular field nodes with equal nodal spacing of h = 0.5 mm were used, while in case 2 a total of 3321 (81×41) regular field nodes with nodal spacing of h = 0.25 mm were used. In addition, 800 rectangular background cells with two-point integration rule were used to perform the Gauss integrations. The step sizes of the incremental displacement were taken as $\Delta u_0 = 0.002$ mm for initial value and $\Delta u = 0.0005$ mm for subsequent loadings until the plate completely looses integrity. Newton–Raphson iteration method was used to solve the non-linear incremental system of governing equations. The convergence of each step was accepted when Eq. (60) was satisfied (Reddy, 2004)

$$\sqrt{\frac{\sum_{I=1}^{N}\left(\underline{u}_I^{(r)} - \underline{u}_I^{(r-1)}\right)^2}{\sum_{I=1}^{N}\left(\underline{u}_I^{(r)}\right)^2}} < 1.0^{-6} \tag{60}$$

The results are shown in Fig. 3 which gives the comparison between two different discretization schemes for the overall axial stress–strain behavior and the damage profile at failure stage along the bottom horizontal boundary of the quarter plate. The results indicate that the two discretization schemes generate nearly identical results, which illustrates the mesh size objectivity of the proposed model.

Fig. 4 shows how the horizontal and vertical displacements evolve at peak and post-peak failure stage corresponding to the imposed displacement levels of-0.0065 mm and-0.0255 mm, corresponding to axial strains of 0.00016 and 0.00064, respectively. Note that, here and in what follows for this example, peak and post-peak failure stages refer to the aforementioned deformation values and negative sign denotes the compression. It can be seen from Fig. 4 that, at peak stress stage, the imperfection has triggered a primitive deformation concentration within the center of the plate as indicated by the darker bands of horizontal and vertical displacements in Fig. 4(a). At the failure post-peak stage, a distinct "hour-glass"-shaped localization band is visible in the vicinity of the small imperfection zone. Note that the "hour-glass" has almost zero displacement in the *x* direction and large outward displacement in the *y* direction. This is expected as the wedges trapped between the shear bands experience near rigid body motions in the *y*-direction as the shear band matures and the plate is compressed in the *x*-direction.

Fig. 5 shows the contours of the axial strain ε_{11} and stress σ_{11} at peak and post-peak failure stages. We also show the vertical strain ε_{22} and stress σ_{22} contours, and the shear strain ε_{12} and stress σ_{12}, in Figs. 6 and 7, respectively, at the peak and post-peak stages. At peak stage shown in Fig. 5(a), the plate deforms almost uniformly except for the visible imperfection zone which shows that the appearance of shear band lags behind the peak stress stage. Upon further loading, a shear band can be observed with an inclination angle of approximately ±45° with respect to the horizontal axis from strain contours in Fig. 5(b). At the same time, a "butterfly" shaped band forms as seen in the stress contour. To further illustrate the evolution of strain as loading progresses, we plot in Fig. 8, the effective strain, calculated as $\varepsilon = \sqrt{(\varepsilon_1)^2 + (\varepsilon_2)^2}$, where ε_1 and ε_2 are the principal strain components, along two horizontal axes (y = 0 and y = 5). Fig. 8 shows clearly that strain localization emerges and grows within a narrow band while the regions outside, which are in elastic state, do not attract further deformation

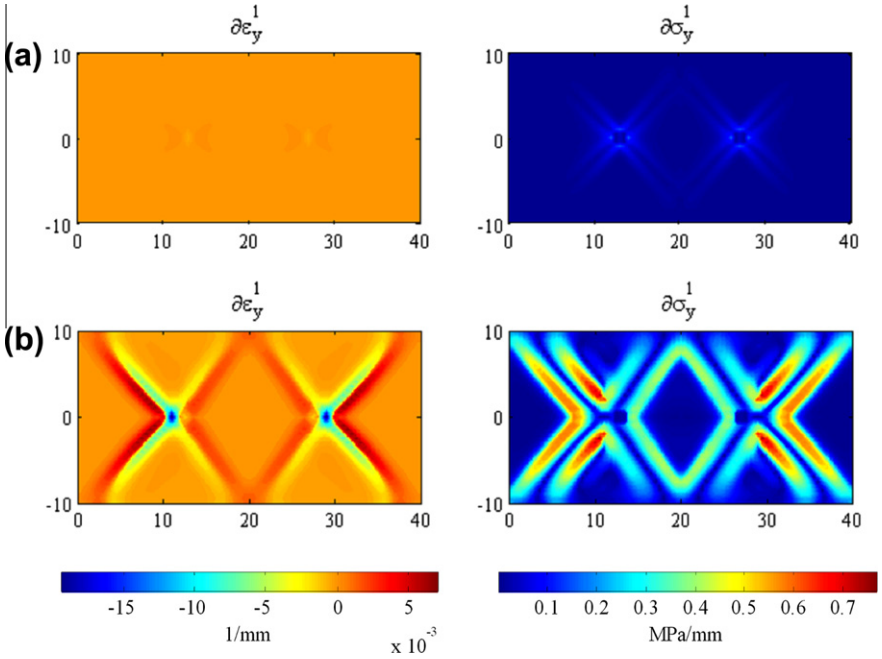

Fig. 15. Contours of the overall effective higher-order strain gradient and conjugated stress in *y*-direction at (a) peak stage and (b) post-peak failure stage.

and even undergo unloading. The shear band formation can be regarded as an interface between two adjacent continua which may be in different deformation state. With this view, it may be possible to use the method presented in this paper to determine the constitutive equations for the two-dimensional nonmaterial interfaces introduced and studied in the papers (dell'Isola and Romano, 1986,1987a,b; dell'Isola and Kosinski, 1993, dell'Isola and Woźniak, 1997a,b).

We also observe that the computed shear band exhibits a tendency to curve in the vicinity of the outer boundaries. This phenomenon may be due to a certain lack of objectivity with respect to the mesh directional bias (Cervera et al., 2004). This mesh directional dependency may come from the shadow integration elements used in the EFG method. Mesh directional bias would be smeared if some true meshfree method were used, such as the modified meshfree local Petrov–Galerkin (MLPG) method presented by Atluri and Zhu (1998). However, it is encouraging that the shear band formation can be predicted using the relatively simple continuum model proposed herein, in which no adaptive analysis is necessary, and therefore, there is no *ad hoc* propagating path for the shear band. Furthermore, the predicted thickness of the shear band is independent of the model discretization and based upon the strain contours can be estimated to be 8–10 mm. Shear bans are also predicted.

Fig. 9 gives the contours of higher-order strain ε_{111} and its conjugate double stress σ_{111} corresponding to the derivatives of the axial strain ε_{11} with respect to the x direction at peak and post-peak failure stages. From Fig. 9(a) we can observe that, at peak stage, both the higher order strain and stress are negligible. However as the shear band forms along the ±45° angle centered on the imperfection zone, strain gradients develop considerably in their proximity as shown in Fig. 9(b). Similarly, the higher-order strain ε_{222} and its conjugate double stress σ_{222} corresponding to the derivatives of the axial strain ε_{22} with respect to the y direction at peak and post-peak failure stages are plotted in Fig. 10.

Fig. 11 illustrates the damage evolution process at selected pre-peak, peak, post-peak pre-failure and failure stages corresponding to the overall displacement levels of (a) −0.006 mm, (b) −0.0065 mm, (c) −0.007 mm, and (d) −0.0255 mm, respectively. The damage initiates from the proximity of the imperfection zone and grows rapidly in an "explosive" manner upon reaching the failure stage. At the same time, the rest of the region experiences zero damage throughout which leads to the homogeneous strains in the remainder of the body. Finally, we note that the shear band thickness as determined by the region in which the damage parameter reaches unity is also 8–10 mm. This thickness is 16 to 20 times the particle radius of 0.5 mm.

5.2. Plate with double imperfections

In the second example we simulate shear band formation in a 2D plate with two equal size imperfections located on the horizontal central axis of the plate. Fig. 12 depicts its original geometry and loading conditions, where hatched area represents the imperfection zones. All the other parameters, material properties and the convergence criterion are taken to be consistent with that for the first example. The step sizes of the incremental displacement were taken as $\Delta u_0 = 0.002$ mm for initial value and $\Delta u = 0.0005$ mm for subsequent loadings until the plate completely fractures.

Fig. 13 shows the contours of the effective strain ε and stress σ at peak and post-peak failure stages corresponding to the overall displacement of −0.007 mm and −0.038 mm. The effective stress is calculated in the same manner as effective strain from the principal stress components σ_1 and σ_2. From Fig. 13(a) one can observe that, at the peak stage, the plate undergoes near homogeneous straining even though primitive shear bands have been formed as shown by the stress contour. When reaching the post-peak failure shown in Fig. 13(b), the two imperfection zones have triggered multiple mature shear bands. It is noticeable that the peripheral shears bands have bigger magnitude than those internal shear bands which could be the result of the interactions between the shear bands. This is also reflected in the stress contours, which are characterized by larger unloading in the outer bands coupled with smaller unloading in the inner bands.

Figs. 14 and 15 give the contours of the overall effective higher-order strain gradients as well as the conjugated double stresses at peak and post-peak failure stages. The effective higher-order

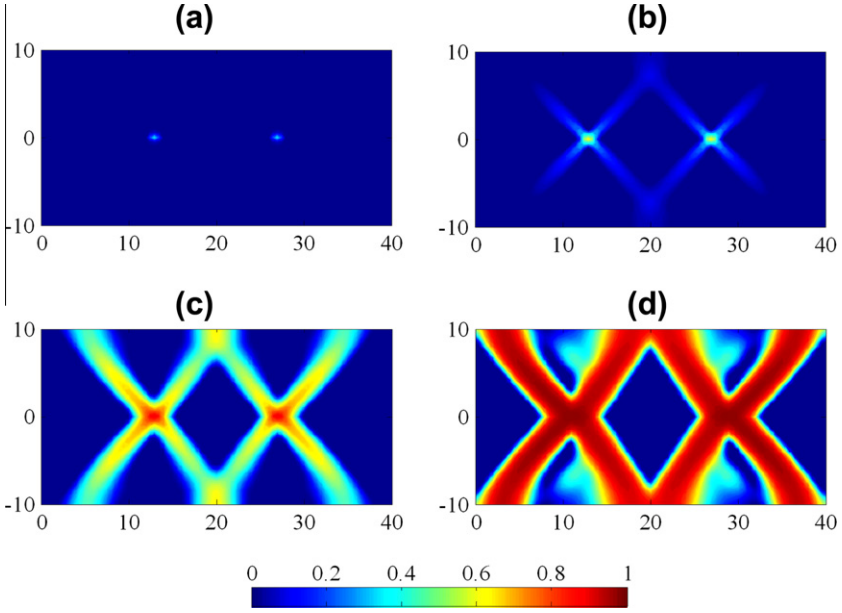

Fig. 16. Evolution process of damage at selected overall displacement levels of (a) −0.006 mm, pre-peak (b) −0.007 mm, peak (c) −0.009 mm, post-peak pre-failure (d) −0.038 mm, post-peak failure.

strains with respect to x- and y-directions, denoted as $\partial\varepsilon_x^1$ and $\partial\varepsilon_y^1$, respectively are evaluated according to

$$\partial\varepsilon_x^1 = \frac{\partial\varepsilon}{\partial x} = \frac{\partial\left(\sqrt{(\varepsilon_1)^2 + (\varepsilon_2)^2}\right)}{\partial x} \tag{61}$$

$$\partial\varepsilon_y^1 = \frac{\partial\varepsilon}{\partial y} = \frac{\partial\left(\sqrt{(\varepsilon_1)^2 + (\varepsilon_2)^2}\right)}{\partial y} \tag{62}$$

Similarly, the corresponding overall effective higher-order stress gradients with respect to x- and y-directions, denoted as $\partial\sigma_x^1$ and $\partial\sigma_y^1$, respectively are calculated from the principal stress components σ_1 and σ_2 according to

$$\partial\sigma_x^1 = \sqrt{\frac{(\sigma_{111})^2 + (\sigma_{221})^2 + 2(\sigma_{121})^2}{2}} \tag{63}$$

$$\partial\sigma_y^1 = \sqrt{\frac{(\sigma_{112})^2 + (\sigma_{222})^2 + 2(\sigma_{122})^2}{2}} \tag{64}$$

The effective higher-order strain gradients are negligible at the peak stress stage. Upon further loading, as one can see from Figs. 14(b) and 15(b), two opposite gradient shear bands form along the either side of the slip line which demonstrates the slope of the strain corresponding to Fig. 13(b). From the effective higher-order stress contour we can also observe a similar pattern of concentration bands which demonstrate the unloading and stress localization respectively. Because of the cross impact, it is expected that inner localization area experiences smaller gradients than that in the outer regions.

Fig. 16 shows the evolution process of damage at selected pre-peak, peak and post-peak pre-failure and post-peak failure stages corresponding to the overall displacement level of (a) −0.006 mm, pre-peak (b) −0.007 mm, peak (c) −0.009 mm, post-peak (d) −0.038 mm, post-peak failure. As seen, the damage progresses smoothly without any numerical difficulties and spurious results, until the damage parameter becomes unity all along the shear band.

6. Concluding remarks

This paper has presented a second gradient stress–strain theory for materials following damage elasticity and successfully applied it to the simulation of shear band localization induced failure problems. The theory was derived in the framework of the method of virtual power which has the advantage of providing an unambiguous formulation with physically meaningful boundary conditions. In contrast to various forms of strain gradient theories, the model proposed herein includes both second gradient strain and conjugated double stress terms such that stable and convergent solutions to the nonlinear problem can be obtained. In addition, the constitutive coefficients for the theory have been derived through a microstructural granular mechanics approach such that internal length scale parameter was introduced directly into the constitutive law with a clear physical foundation.

The derived model can reproduce the shear band propagation without any *ad hoc* information which indicates that this method will be suitable for modeling more complex crack propagation problems. Although a minor subjectivity with respect to mesh directional bias have been observed at the outer lateral boundaries of the 2D plate examples, the two numerical examples results are encouraging considering that (a) we adopted the "shadow mesh" necessitated EFG method, and (2) we did not use any kind of adaptive procedure (neither h-adaptivity nor p-adaptivity) for which the propagating paths are required a priori. The comparison of results between two different discretization schemes shown in the first example indicate that the mesh-size dependency has been overcame. In our future work, we will implement this higher-order continuum theory into other truly mesh-free methods as well as employ further refinements in our constitutive laws.

Acknowledgements

This research is supported in part by the United States National Science Foundation Grant CMMI-1068528 (AM).

References

Adachi, T., Oka, F., Yashima, A., 1991. A finite element analysis of strain localization for soft rock using a constitutive equation with strain softening. Applied Mechanics 61 (3), 183–191.

Alibert, J.J., Seppecher, P., dell'Isola, F., 2003. Truss modular beams with deformation energy depending on higher displacement gradients. Mathematics and Mechanics of Solids 8 (1), 51–73.

Altan, B.S., Aifantis, E.C., 1997. On some aspects in the special theory of gradient elasticity. Journal of the Mechanical Behavior of Materials 8, 231–282.

Armero, F., Garikipati, K., 1995. Recent advances in the analysis and numerical simulation of strain localization in inelastic solids. In: Owen, D., Onate, E., Hinton, E. (Eds.), Computational Plasticity, Fundamentals and Applications. pp. 547–561.

Armero, F., Garikipati, K., 1996. An analysis of strong discontinuities in multiplicative finite strain plasticity and their relation with the numerical simulation of strain localization in solids. International Journal of Solids and Structures 33 (20–22), 2863–2885.

Askes, H., Pamin, J., de Borst, R., 2000. Dispersion analysis and element-free Galerkin solutions of second- and fourth-order gradient enhanced damage models. International Journal for Nu-merical Methods in Engineering 49, 811–832.

Atluri, S.N., Zhu, T., 1998. A new Meshless Local Petrov-Galerkin (MLPG) approach in computational mechanics. Computational Mechanics 22, 117–127.

Bažant, Z.P., 1976. Instability, ductility, and size effect in strain-softening concrete. Journal of the Engineering Mechanics Division 102 (2), 331–344.

Bažant, Z.P., Belytschko, T., Chang, T.P., 1984. Continuum theory for strain-softening. Journal of Engineering Mechanics 110 (2), 666–1692.

Bažant, Z.P., Pijaudier-Cabot, G., 1988. Nonlocal continuum damage, localization instability and convergence. Journal of Applied Mechanics 55, 287–293.

Belytschko, T.B., Bažant, Z.P., Hyun, Y.W., Chang, T.P., 1986. Strain-softening materials and finite-element solutions. Computers and Structures 23 (2), 163–180.

Belytschko, T., Fish, J., Englemann, B., 1988. A finite element method with embedded localization zones. Computer Methods in Applied Mechanics and Engineering 70, 59–89.

Belytschko, T., Gu, L., Lu, Y.Y., 1994a. Fracture and crack growth by element free Galerkin methods. Modeling and Simulation in Materials Science and Engineering 2 (3A), 519–534.

Belytschko, T., Lu, Y.Y., Gu, L., 1994b. Element-free Galerkin methods. International Journal for Numerical Methods in Engineering 37 (2), 229–256.

Belytschko, T., Lu, Y.Y., Gu, L., 1995a. Crack propagation by element-free Galerkin methods. Engineering Fracture Mechanics 51 (2), 295–315.

Belytschko, T., Lu, Y.Y., Gu, L., Tabbara, M., 1995b. Element-free Galerkin methods for static and dynamic fracture. International Journal of Solids and Structures 32 (17–18), 2547–2570.

Belytschko, T., Tabbara, M., 1996. Dynamic fracture using element-free Galerkin methods. International Journal for Numerical Methods in Engineering 39, 923–938.

Bigoni, D., Hueckel, T., 1991. Uniqueness and localization-I. Associative and non-associative elastoplasticity. International Journal of Solids and Structures 28, 197–213.

Borja, R.I., Regueiro, R.A., Lai, T.Y., 2000. FE modelling of strain localization in soft rock. Journal of Geotechnical Geoenvironmental Engineering 126 (4), 335–343.

Callari, C., Armero, F., Abati, A., 2010. Strong discontinuities in partially saturated poroplastic solids. Computer Methods in Applied Mechanics and Engineering 199 (23–24), 1513–1535.

Cervera, M., Chiumenti, M., de Saracibar, A., 2004. Shear band localization via local J2 continuum damage mechanics. Computer Methods in Applied Mechanics and Engineering 193 (9–11), 849–880.

Chambon, R., Caillerie, D., El Hassan, N., 1998. One-dimensional localization studied with a second grade model. European Journal of Mechanics A/Solids 17, 637–656.

Chang, C.S., Askes, H., Sluys, L.J., 2002. Higher-order strain/higher-order stress gradient models derived from a discrete microstructure, with application to fracture. Engineering Fracture Mechanics 69, 1907–1924.

Chang, C.S., Gao, J., 1995. Second-gradient constitutive theory for granular material with random packing structure. International Journal of Solids and Structures 32 (16), 2279–2293.

Chang, C.S., Gao, J., 1997. Wave propagation in granular rod using high-gradient theory. ASCE: Journal of Engineering Mechanics 123, 52–59.

Chang, C.S., Gao, J., Zhong, X., 1998. High-gradient modeling for love wave propagation in geological materials. ASCE: Journal of Engineering Mechanics 124, 1354–1359.

Chang, C.S., Liao, C.L., 1990. Constitutive relation for a particulate medium with the effect of particle rotation. International Journal of Solids and Structures 26 (4), 437–453.

Chang, C.S., Ma, L., 1990. Modeling of discrete granulates as micropolar continua. Journal of Engineering Mechanics 116 (12), 2703–2721.

Chang, C.S., Misra, A., 1989. Computer simulation and modelling of mechanical properties of particulates. Computer and Geotechnics 7 (4), 262–287.

Chang, C.S., Misra, A., 1990. Packing structure and mechanical properties of granulates. ASCE: Journal of Engineering Mechanics 116 (5), 1077–1093.

Chang, C.S., Wang, T.K., Sluys, L.J., van Mier, J.G.M., 2002a. Fracture modeling using a micro-structural mechanics approach-I. Theory and formulation. Engineering Fracture Mechanics 69, 1941–1958.

Chang, C.S., Wang, T.K., Sluys, L.J., van Mier, J.G.M., 2002b. Fracture modeling using a micro-structural mechanics approach-II. Finite Element Analysis. Engineering Fracture Mechanics 69, 1959–1976.

Chen, J.S., Wu, C.T., Belytschko, T., 2000. Regularization of material instabilities by meshfree approximations with intrinsic length scales. International Journal for Numerical Methods in Engineering 47, 1303–1322.

Cordes, L.W., Moran, B., 1996. Treatment of material discontinuity in the Element-Free Galerkin method. Computer Methods in Applied Mechanics and Engineering 139, 75–89.

de Borst, R., Mühlhaus, H.B., 1992. Gradient-dependent plasticity: Formulation and algorithmic aspects. International Journal for Numerical Methods in Engineering 35, 21–39.

de Borst, R., Sluys, L.J., Mühlhaus, H.B., Pamin, J., 1993. Fundamental issues in finite element analyses of localization of deformation. Engineering Computations 10, 99–121.

de Borst, R., Pamin, J., Peerlings, R.H.J., Sluys, L.J., 1995. On gradient-enhanced damage and plasticity models for failure in quasi-brittle and frictional materials. Computational Mechanics 17 (1–2), 130–142.

de Borst, R., Gutiérrez, M.A., Wells, G.N., Remmers, J.J.C., Askes, H., 2004. Cohesive-zone models, higher-order continuum theories and reliability methods for computational failure analysis. International Journal for Numerical Methods in Engineering 60, 289–315.

dell'Isola, F., Romano, A., 1986. On a general balance law for continua with an interface. Ricerche di Matematica 35, 325–337.

dell'Isola, F., Romano, A., 1987a. On the derivation of thermomechanical balance equations for continuous systems with a nonmaterial interface. International Journal of Engineering Science 25, 1459–1468.

dell'Isola, F., Romano, A., 1987b. A phenomenological approach to phase transition in classical field theory. International Journal of Engineering Science 25, 1469–1475.

dell'Isola, F., Kosinski, W., 1993. Deduction of thermodynamic balance laws for bidimensional nonmaterial directed continua modelling interphase layers. Archives of Mechanics 45, 333–359.

dell'Isola, F., Seppecher, P., 1995. The relationship between edge contact forces, double force and interstitial working allowed by the principle of virtual power. Comptes Rendus de l'Academie de Sciences–Serie IIb: Mecanique, Physique, Chimie, Astronomie 321, 303–308.

dell'Isola, F., Seppecher, P., 1997. Edge contact forces and quasi-balanced power. Meccanica 32, 33–52.

dell'Isola, F., Woźniak, C., 1997a. On phase transition layers in certain micro-damaged two-phase solids. International Journal of Fracture 83, 175–189.

dell'Isola, F., Woźniak, C., 1997b. On continuum modelling the interphase layers in certain two-phase elastic solids. Zeitschrift fur Angewandte Mathematik und Mechanik 77, 519–526.

dell'Isola, F., Madeo, A., Seppecher, P., 2009. Boundary conditions at fluid permeable interfaces in porous media: a variational approach. International Journal of Solids and Structures 46, 3159–3164.

dell'Isola, F., Madeo, A., Placidi, L. 2011. Linear plane wave propagation and normal transmission and reflection at discontinuity surfaces in second gradient 3D continua. Zeitschrift für Angewandte Mathematik und Mechanik. <http://dx.doi.org/10.1002/zamm.201100022>.

dell'Isola, F., Seppecher, P., Madeo, A. 2012. How contact interactions may depend on the shape of Cauchy cuts in Nth gradient continua: approach "a la D'Alembert". Zeitschrift für Angewandte Mathematik und Physik (ZAMP). <http://dx.doi.org/10.1007/s00033-012-0197-9>.

de Vree, J.H.P., Brekelmans, W.A.M., van Gils, M.A.J., 1995. Comparison of nonlocal approaches in continuum damage mechanics. Computers and Structures 55, 581–588.

Di Prisco, C., Imposimato, S., 2003. Nonlocal numerical analyses of strain localisation in dense sand. Mathematical and Computer Modelling 37 (5–6), 497–506.

Fish, J., Belytschko, T., 1988. Elements with embedded localization zones for large deformation problems. Computers & Structures 30 (1–2), 247–256.

Fleck, N.A., Hutchinson, J.W., 1997. Strain gradient plasticity. Advances in Applied Mechanics 33, 295–361.

Frantziskonis, G., Desai, C.S., 1987. Analysis of a strain softening constitutive model. International Journal of Solids and Structures 23 (6), 751–767.

Germain, P., 1973. The method of virtual power in continuum mechanics. Part 2: Microstructure. SIAM Journal of Applied Mathematics 25 (3), 556–575.

Jirásek, M., 1998. Element-free Galerkin method applied to strain-softening materials. In: R. de Borst et al. (Eds.), Proceedings of EURO-C, International Conference Computational Modelling of Concrete Structures 1(A.A.) Balkema, Rotterdam/Brookfield. pp. 311–319.

Khoei, A.R., Bakhshiani, A., 2005. A hypoelasto-viscoplastic endochronic model for numerical simulation of shear band localization. Finite Elements in Analysis and Design 41 (14), 1384–1400.

Krysl, P., Belytschko, T., 1995. Analysis of thin plates by the elementfree Galerkin method. Computational Mechanics 17 (1/2), 26–35.

Krysl, P., Belytschko, T., 1997. Propagation of 3D cracks by the element free Galerkin method. Fourth U.S. National Congress on Computational Mechanics, San Francisco.

Krysl, P., Belytschko, T., 1999. The element free galerkin method for dynamic propagation of arbitrary 3-D cracks. International Journal for Numerical Methods in Engineering 44 (6), 767–800.

Larsson, R., Runesson, K., Sture, S., 1996. Embedded localization band in undrained soil based on regularized strong discontinuity theory and finite element analysis. International Journal of Solids and Structures 33 (20-22), 3081–3101.
Lemaitre, J., Chaboche, J.L., 1990. Mechanics of Solid Materials. Cambridge University Press, Cambridge U.K.
Li, S., Liu, W.K., Rosakis, A.J., Belytschko, T., Hao, W., 2002. Mesh free galerkin simulations of dynamic shear band propagation and failure mode transition. International Journal of Solids and Structures 39, 1213–1240.
Li, S., Liu, W.K., 2004. Simulations of strain localization. In: Meshfree Particle Methods. Springer, New York, pp. 201–215.
Liu, G.R., Gu, Y.T., 2005. An Introduction to Meshfree Methods and Their Programming. Springer, New York, Dordrecht.
Lu, Y.Y., Belytschko, T., Tabbara, M., 1994. Element-free Galerkin methods for wave propagation and dynamic fracture. Computer methods in Applied Mechanics and Engineering 126 (1–2), 131–153.
Manzari, M.T., 2004. Application of micropolar plasticity to post failure analysis in geomechanics. International Journal for Numerical and Analytical Methods in Geomechanics 28 (10), 1011–1032.
Misra, A., Yang, Y., 2010. Micromechanical model for cohesive materials based upon pseudo-granular structure. International Journal of Solids and Structures 47, 2970–2981.
Mohan, L.S., Nott, P.R., Rao, K.K., 2002. A frictional Cosserat model for the slow shearing of granular materials. Journal of Fluid Mechanics 457, 377–409.
Mukherjee, Y.X., Mukherjee, S., 1997. On boundary conditions in the element-free Galerkin method. Computational Mechanics 19, 264–270.
Murakami, H., Kendall, D.M., Valanis, K.C., 1993. A nonlocal elastic damage theory: mesh-insensitivity under strain softening. Computers and Structures 48 (3), 415–422.
Mühlhaus, H.B., Oka, F., 1996. Dispersion and wave propagation in discrete and continuous models for granular materials. International Journal of Solids and Structures 33, 2841–2858.
Needleman, A., 1988. Material rate dependence and mesh sensitivity in localization problems. Computer Methods in Applied Mechanics and Engineering 67, 69–85.
Nemes, J.A., Spéciel, E., 1996. Use of a rate-dependent continuum damage model to describe strain-softening in laminated composites. Computers and Structures 58 (6), 1083–1092.
Oliver, J., Cervera, M., Manzoli, O., 1997. On the use of J2 plasticity models for the simulation of 2D strong discontinuities in solids. In: Owen, D., Onate, E., Hinton, E. (Eds.), Proc. Int. Conf. on Computational Plasticity. CIMNE, Barcelona, Spain, pp. 38–55.
Oliver, J., Cervera, M., Manzoli, O., 1998. On the use of strain-softening models for the simulation of strong discontinuities in solids. In: de Borst, R., van der Giessen, E. (Eds.), Material Instabilities in Solids. John Wiley & Sons, pp. 107–123, Chapter 8.
Oliver, J., Cervera, M., Manzoli, O., 1999. Strong discontinuities and continuum plasticity models: the strong discontinuity approach. International Journal of Plasticity 15, 319–351.
Oliver, J., Huespe, A.E., Samaniego, E., 2003. A study on finite elements for capturing strong discontinuities. International Journal for Numerical Methods in Engineering 56, 2135–2161.
Ortiz, M., Leory, Y., Needleman, A., 1987. A finite element method for localized failure analysis. Computer Methods in Applied Mechanics and Engineering 61 (2), 189–214.
Pamin, J., 1994. Gradient-dependent plasticity in numerical simulation of localization phenomena. Ph.D. Thesis, Delft University of Technology, The Netherlands.
Pamin, J., Askes, H., de Borst, R., 2001. Gradient regularization and EFG discretization of the plastic flow theory. In: Bletzinger, K.-U., Schweizerhof, K., Wall, W.A. (Eds.), Conference on Trends in Computational Structural Mechanics. CIMNE, Barcelona, pp. 179–188.
Pamin, J., Askes, H., de Borst, R., 2003. Two gradient plasticity theories discretized with the element-free Galerkin method. Computer Methods in Applied Mechanics and Engineering 192, 2377–2403.
Peerlings, R.H.J., de Borst, R., Brekelmans, W.A.M., de Vree, J.H.P., 1996. Gradient enhanced damage for quasi-brittle materials. International Journal for Numerical Methods in Engineering 39 (19), 3391–3403.
Pietruszczak, St., Mroz, Z., 1981. Finite element analysis of deformation of strain-softening materials. International Journal for Numerical Methods in Engineering 17, 327–334.
Rabczuk, T., Areias, P.M.A., Belytschko, T., 2000. A simplified meshfree method for shear bands with cohesive surfaces. International Journal for Numerical Methods in Engineering 00, 1–6.
Rabczuk, T., Belytschko, T., 2005. Adaptivity for structured meshfree particle methods in 2D and 3D. International Journal for Numerical Methods in Engineering 63, 1559–1582.
Rajesh, K.N., Rao, B.N., 2010. Coupled meshfree and fractal finite element method for mixed mode two-dimensional crack problems. International Journal for Numerical Methods in Engineering 84, 572–609.
Reddy, J.N., 2004. An Introduction to Nonlinear Finite Element Analysis. Oxford University Press, New York.
Reddy, J.N., 2005. An Introduction to Finite Element Method, third ed. McGraw-Hill Science/Engineering/Math.
Regueiro, R.A., Lai, T.Y., Borja, R.I., 1998. Computational modelling of strain localization in soft rock. In: Evangelista, A., Picarelli, L. (Eds.), Geotechnics of Hard Soils-Soft Rocks. The Netherlands, Balkema, Rotterdam, pp. 789–797.
Regueiro, R.A., Borja, R.I., 1999. A finite element model of localized deformation in frictional materials taking a strong discontinuity approach. Finite Elements in Analysis and Design 33 (4), 283–315.
Rice, J.R., 1977. The localization of plastic deformation. In: Koiter, W.T. (Ed.), Theoretical and Applied Mechanics. North-Holland, Amsterdam, pp. 207–220.
Rudnicki, J.W., 1977. The inception of failure in a rock mass with a weakened zone. Journal of Geophysical Research 82 (5), 844–854.
Samaniego, E., Belytschko, T., 2005. Continuum-discontinuum modelling of shear bands. International Journal for Numerical Methods in Engineering 62 (13), 1857–1872.
Seppecher, P., Alibert, J.-J., dell'Isola, F., 2011. Linear elastic trusses leading to continua with exotic mechanical interactions. Journal of Physics: Conference Series 319 (1), 012018.
Sluys, L.J., de Borst, R., Mühlhaus, H.B., 1993. Wave propagation, localization and dispersion in a gradient-dependent medium. International Journal of Solids and Structures 30, 1153–1171.
Sandler, I.S., 1984. Strain softening for static and dynamic problems. ASME Winter Annual Meeting, Symp. On Constitutive Equations: Micro, Macro and Computational Aspects, CEQ. New Orleans, 217–231.
Simo, J., Oliver, J., 1994. A new approach to the analysis and simulation of strong discontinuities. In: Bazant, Z.B., Bittnar, Z., Jirasek, M., Mazars, J. (Eds.), Fracture and Damage in Quasi-brittle Structures. E & FN Spon, pp. 25–39.
Simo, J., Oliver, J., Armero, F., 1993. An analysis of strong discontinuities induced by strain-softening in rate-independence inelastic solids. Computational Mechanics 12, 277–296.
Sluys, L.J., 1992. Wave propagation, localization and dispersion in softening solids. Ph.D. Thesis, Delft University of Technology, The Netherlands.
Sluys, L.J., de Borst, R., 1992. Wave-propagation and localization in a rate-dependent cracked medium model formulation and one-dimensional examples. International Journal of Solids and Structures 29, 2945–2958.
Steinmann, P., 1994. An improved FE expansion for micropolar localization analysis. Communications in Numerical Methods in Engineering 10 (12), 1005–1012.
Su, X.M., 1994. Strain localization in plane strain micropolar elasticity. Archive of Applied Mechanics 64 (4), 258–266.
Suiker, A.S.J., de Borst, R., Chang, C.S., 2001a. Micro-mechanical modeling of granular material. Part 1-Derivation of a second-gradient micro-polar constitutive theory. Acta Mechanica 149 (1–4), 161–180.
Suiker, A.S.J., de Borst, R., Chang, C.S., 2001b. Micro-mechanical modeling of granular material. Part 2-Plane wave propagation in infinite media. Acta Mechanica 149 (1–4), 181–200.
Triantafyllidis, N., Bardenhagen, S., 1993. On higher order gradient continuum theories in 1-D nonlinear elasticity. Derivation from and comparison to the corresponding discrete models. Journal of Elasticity 33, 259–293.
Valanis, K.C., 1991. A global damage theory and the hyperbolicity of the wave problem. ASME Journal of applied Mechanics 58 (2), 311–316.
Wu, F.H., Freund, L.B., 1984. Deformation trapping due to thermoplastic instability in one dimensional wave propagation. Journal of Mechanics and Physics of Solids 32 (2), 119–132.
Yagawa, G., 2004. Node-by-node parallel finite elements: a virtually meshless method. International Journal for Numerical Methods in Engineering 60, 69–102.
Yang, Y., Misra, A., 2010. Higher-order stress-strain theory for damage modeling implemented in an element-free Galerkin formulation. Computer Modeling in Engineering and Sciences 64 (1), 1–36.
Yang, Y., Ching, W.Y., Misra, A., 2011. Higher-order continuum theory applied to fracture simulation of nano-scale intergranular glassy film. Journal of Nanomechanics and Micromechanics 1, 60–71.
Zhang, Y.Y., Gao, L.S., 2010. A simplified meshless method for cohesive cracks. International Journal for Numerical Methods in Biomedical Engineering 26, 728–739.
Zhao, J., Sheng, D., Zhou, W., 2005. Shear banding analysis of geomaterials by strain gradient enhanced damage model. International Journal of Solids and Structures 42 (20), 5335–5355.